Biomaterials Science

ROYAL SOCIETY OF CHEMISTRY

REVIEW

Cite this: *Biomater. Sci.*, 2024, **12**, 4506

Design considerations and biomaterials selection in embedded extrusion 3D bioprinting†

Swaprakash Yogeshwaran,[a] Hossein Goodarzi Hosseinabadi,[b,c] Daniel E. Gendy[a] and Amir K. Miri *[a]

Received 21st April 2024,
Accepted 11th July 2024

DOI: 10.1039/d4bm00550c

rsc.li/biomaterials-science

In embedded extrusion 3D bioprinting, a temporary matrix preserves a paste-like filament ejecting from a narrow nozzle. For granular sacrificial matrices, the methodology is known as the freeform reversible embedding of suspended hydrogels (FRESH). Embedded extrusion 3D bioprinting methods result in more rapid and controlled manufacturing of cell-laden tissue constructs, particularly vascular and multi-component structures. This report focuses on the working principles and bioink design criteria for implementing conventional embedded extrusion and FRESH 3D bioprinting strategies. We also present a set of experimental data as a guideline for selecting the support bath or matrix. We discuss the advantages of embedded extrusion methods over conventional biomanufacturing methods. This work provides a short recipe for selecting inks and printing parameters for desired shapes in embedded extrusion and FRESH 3D bioprinting methods.

1. Introduction

Biofabrication technologies allow the creation of 3D *in vitro* biomimetic models with the complexity of tissues and organs.[1,2] 3D bioprinting includes an automated deposition of cells, spheroids, or multi-cellular organoids embedded in bioinks based on a predefined computer-aided design model.[3] The current challenges in 3D bioprinting involve cell sourcing, vascularized modeling, creating thick constructs, improving surface artifacts, and ensuring processing safety.[4,5] Embedded extrusion 3D bioprinting can make high aspect-ratio constructs at a proper resolution at a clinically relevant scale.[6] This method uses a shear-thinning material, such as gelatin, as a temporary bath or matrix,[7] which preserves the filament shape. The shortage of shear-thinning reversible hydrogels has limited the growth of embedded extrusion 3D bioprinting. In response to this challenge, freeform reversible embedding of suspended hydrogels (FRESH) has been proposed by making a granular matrix.[8] The support matrix can be quickly melted or removed, leaving behind the desired 3D tissue or the whole organ.[9]

Embedded 3D bioprinting uses low-viscosity bioinks such as collagen, alginate, hyaluronic acid (HA), and fibrin to produce vascular, kidney, brain, heart, and other biomimetic models.[6] Embedded extrusion 3D bioprinting can be classified into granular (*i.e.*, FRESH) and non-granular matrices. The FRESH strategy enables using a broad range of synthetic polymer bioinks, such as epoxies,[10] silicones,[11] urethanes,[10] and photoresist,[12] when paired with a suitable support matrix. The principles of embedded extrusion 3D bioprinting are illustrated in Fig. 1A, and different types of bioink, crosslinking routes, paths for printing, and support matrix compositions are summarized in Fig. 1B. The FRESH uses shaped microparticles created by the mechanical blending of a large gelatin block. Lee *et al.*[13] developed a coacervation approach to generate gelatin microparticles with (i) uniform spherical morphology, (ii) reduced polydispersity, and (iii) decreased particle diameter around ~25 μm.

In this work, we reviewed existing embedded extrusion 3D bioprinting methods. We provided a handy guide for developing an appropriate granular matrix using the experimental results on two well-used matrices: gelatin and agarose. We also made master curves to summarize the rheological landscape for the support matrix, which can be converted into the extracellular matrix (ECM) in the final product. After summarizing fundamental working principles and ink design criteria for implementing the strategy, this review highlighted the advantages of embedded extrusion or FRESH strategies over traditional extrusion-based techniques across a spectrum of biomedical applications.

[a]*Department of Biomedical Engineering, Newark College of Engineering, New Jersey Institute of Technology, 323 Dr Martin Luther King Jr Blvd, Newark, NJ 07102, USA. E-mail: am3296@njit.edu; Tel: +973-596-6366*
[b]*Institute of Pharmacology and Toxicology, University Medical Center Göttingen, Robert-Koch-Str. 40, 37075 Göttingen, Germany*
[c]*Department of Biomedical Engineering, Eindhoven University of Technology, 5600 MB Eindhoven, The Netherlands*

† Electronic supplementary information (ESI) available. See DOI: https://doi.org/10.1039/d4bm00550c

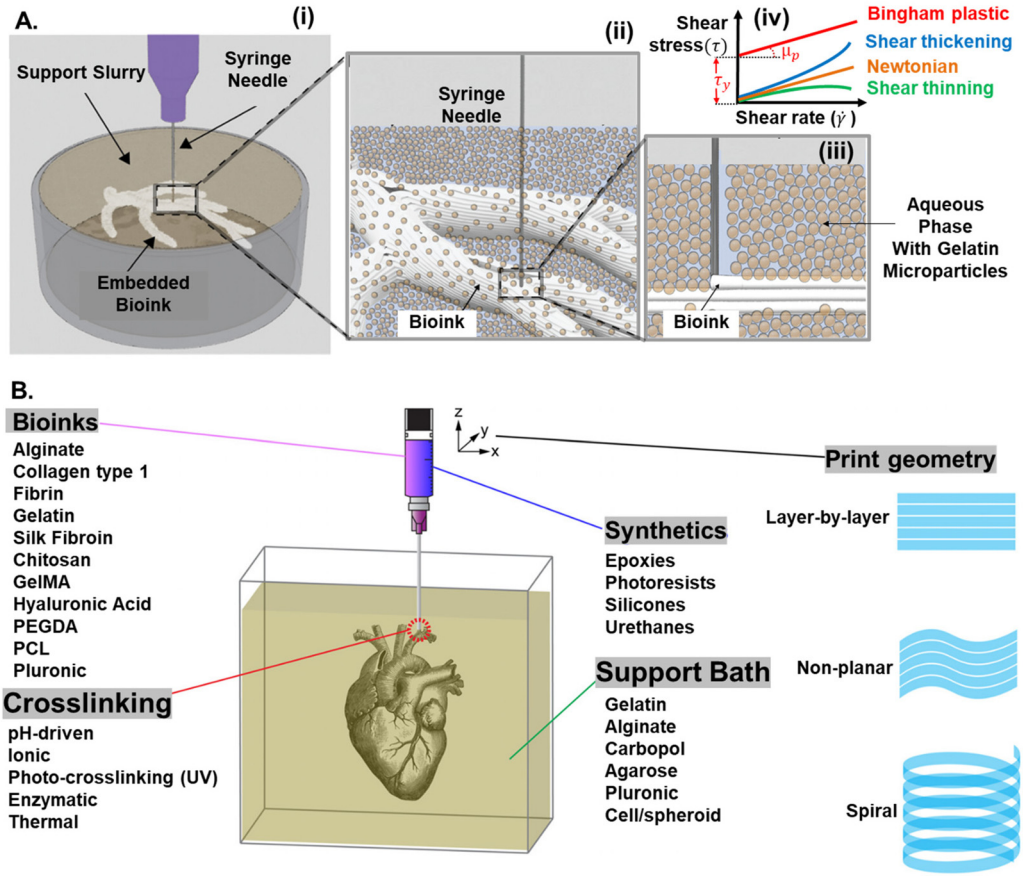

Fig. 1 Embedded extrusion 3D bioprinting: (A) A print container is filled with a yield-stress gel microparticle support matrix to serve as the embedding medium for the intended components (i), the aqueous phase of the support matrix can be tuned to drive crosslinking/gelation of the nozzle-extruded bioink as the microparticles support the print during layer-by-layer deposition (ii), as the needle moves through the support matrix, the microparticles yield providing a space for the extruded bioink and subsequently heal behind the needle providing support to the curing bioink (iii); the flow behavior of the support bath is Bingham plastic (iv). (B) Classification of different synthetic or natural bioinks, different crosslinking routes, different paths for printing, and matrix compositions (adapted from ref. 9 with permission from AIP Publishing, copyright 2021).

2. Principles of embedded extrusion 3D bioprinting

2.1. Support bath preparation

Shear-thinning biomaterials, such as various yield-stress fluids, can be used as the support matrix. The surface properties of the matrix material enable their selection as the support matrix. Hydrophilic shear-thinning materials for the support matrix include gellan, gelatin, alginate, agarose, Carbopol, and nano-clay (LAPONITE®). Hydrophobic support matrix materials include silicone elastomers, fumed silica in oils, and micro-organogels, whereas amphiphilic support materials such as Pluronic F127 have been used owing to their unique interfacial characteristics.[14] Hinton *et al.* demonstrated the 3D printing of hydrophobic polydimethylsiloxane (PDMS) prepolymer resins within a hydrophilic Carbopol gel support *via* freeform reversible embedding.[15] In this method, the Carbopol support acts as a Bingham plastic that yields and shows fluidity during extrusion. A combination of the immiscibility of hydrophobic PDMS and hydrophilic Carbopol was used to maintain dimensional stability. The Carbopol support gel then releases the embedded PDMS prints using a phosphate-buffered saline solution to reduce the Carbopol yield stress. Rocca *et al.* developed multi-material embedded extrusion 3D bioprinting[16] where the supporting matrix relied on a thermo-responsive biomaterial, Pluronic F127, with a reversible sol–gel phase transition temperature of around 4 °C.[17]

Bingham plastic-like rheology allows a laminar flow of the 3D printing bioink. In contrast to fluids with conventional Newtonian, shear thinning, or shear thickening responses, a support bath behaves as a solid till a certain shear stress loading, as shown in Fig. 1Aiv. Newtonian fluids have a viscosity (μ_n), where the shear stress (τ_n) and shear rate ($\dot{\gamma}_n$) are linearly related by the equation $\tau_n = \mu_n \cdot \dot{\gamma}_n$. Bingham plastic has a plastic viscosity (μ_p), where the shear stress (τ_p) and shear rate ($\dot{\gamma}_p$) are related by the equation $\tau_p = \tau_y + \mu_p \cdot \dot{\gamma}_p$. In this definition, τ_y is the yield point or the stress threshold, and the material will flow proportionally to the applied shear above τ_y. Maintaining shape fidelity when printing into a suspension

medium.[18] The Bingham plastic matrix provides rigid support to the extruded bioink while instantly yielding and recovering during and after the passage of the nozzle.[19–22] The Bingham plastic response describes the property of certain materials that act as solids until shear forces exceed a threshold, which causes the material to transition and have liquid-like behavior, thus allowing a thin nozzle to move freely through the matrix. Indeed, the granular support matrix with compacted microparticles behaves as Bingham plastic[23] and solidifies after the nozzle deposition. This approach has been demonstrated by depositing liquid hydrogel precursors within self-healing support materials.[15,24–28]

Patricio *et al.* reported a widely available and cost-effective natural polymer based on xanthan gum with a high molecular weight that provides high viscosity at low shear rates for a sacrificial support matrix.[29] Bulk hydrogel based on reversible physical crosslinking, such as host–guest HA[30] shows the required shear-thinning pseudo-plasticity to be used as support matrices, and its continuous matrix ensures improved printing resolution compared to granular systems. The resolution, size, and 3D architecture of produced tissue models can be adjusted, while enzymatic cleavage or mechanical separation can be employed for bath removal. Embedded extrusion 3D bioprinting is better suited for thick structures and composite models than other methods.

Non-embedded extrusion methods such as light-assisted 3D printing, Inkjet 3D printing, and conventional extrusion-based methods distort the soft and liquid-like bioinks due to gravity, causing subsequent loss of fidelity and collapsing the structure. Without physical support, most bioinks are challenging to print layer-by-layer and cannot cure or crosslink quickly enough with sufficient rigidity to allow for structure stability.[31] The embedded environment provides physical support for 3D shapes. Some commonly used bioink-support matrix combinations and their applications are listed below in Table 1.

2.2. 3D bioprinting parameters

The friction forces between the filament and the support matrix help the nozzle stability[31] (Fig. 1Aiii). To maintain cell viability, the matrix should be sterile, aqueous, and supplemented with buffers in its aqueous phase. The design parameters are (I) optimal yield stress, (II) printing speed, and (III) nozzle size. The optimal yield stress depends on the needle diameter, print speed, and biomaterials. The syringe needle diameter affects print resolution and feature size. Smaller (*e.g.*, <100 μm) nozzles allow higher-resolution prints with increased print time. Larger nozzles (*e.g.*, >100 μm) increase printing speed (~50 mm s^{-1}) due to increased layer height and filament width but decrease printing resolution. Smaller needle diameters necessitate slower printing speed (~10 mm s^{-1}).[43]

2.3. Biophysical properties of support matrix

The microparticle concentration in the granular matrix affects its mechanical properties and the printability of the extruded materials.[44] Higher concentrations provide more structural support and increase the viscosity (*i.e.*, resistance to deposition). Lower concentrations offer better printability but compromise the mechanical stability. Gelatin concentrations of 4.5% w/v (in 0.125% w/v $CaCl_2$ when alginate is a part of the bioink system) are used to make the gelatin matrix, but the optimal concentration can vary depending on the specific bioink and printing conditions.

The cooling rate and microparticle density can adjust the gelation temperature for gelatin. Agarose gelation is around 28–36 °C, and gelatin occurs at around 22–25 °C. Different microparticle sources can have varying gelation temperatures and swelling properties, affecting the gel strength. For example, the gelatin microparticle matrix at 4.5% w/v concentration behaves like Bingham plastic at low temperatures and a more viscous liquid above 37 °C. This thermo-reversible behavior makes gelatin an ideal support matrix for the embedded extrusion and FRESH 3D bioprinting.[31] The mechanical resistance offered by the matrix provides immediate support and structural stability to the extruded print.

Another parameter is the presence of a chemical or enzymatic crosslinker. Crosslinkers improve the extruded material's stability while maintaining print fidelity. After the extrusion process, the support matrix is melted at 37 °C while

Table 1 Common bioink-support matrix combinations for embedded extrusion 3D bioprinting

Support type	Support matrix	Bioink	Application	Ref.
Granular	Alginate microparticles in xanthan gum	Sacrificial gelatin	Vascularized heart model	32
	κ-Carrageenan (CarGrow)	Fibrin	Bone- and cardiac- constructs	33
	Agarose gel microparticles	Collagen, gellan gum, alginate, and i-Carrageenan	Carotid artery, T7 invertebral disc	34
	Alginate microparticles in collagen & hyaluronic acid	Stem cells & sacrificial gelatin	Neural models, vascular-like channel	35
	Carbopol microparticles	Gelatin methacryloyl (GelMA)	*In vitro* (neuroblastoma) model	36
Non-granular	Cellulose nanocrystals (CNC)	Gelatin, GelMA, alginate, platelet lysate, Pluronic F-127	Tumor-on-a-chip model, *in vitro* tendon model	37
	Oxidize bacterial cellulose	Poly-L-lysine	*In vitro* vessel model	38
	Poly(ethylene oxide)-rich matrix after phase separation	Poly (acrylic acid), dextran	On-demand *in vitro* tissue model	39
	An organ building block based ECM	iPSCs and sacrificial gelatin	Perfusable cardiac tissues	40
	Skin derived dECM	Vascular tissue-derived dECM	*In vitro* melanoma model	41
	Vascular tissue derived dECM	Calcium-Pluronic F127	*In vitro* atherosclerotic model	42

the printed bioink material undergoes gelation. This reversible property of the extruded material is another parameter that makes embedded extrusion efficient for making soft biomaterials. The support matrix generally comprises gelatin or agarose microparticles that behave as a Bingham plastic or Herschel–Bulkley fluid, where it is a solid until sufficient shear stress is applied, after which point it starts to develop liquid-like behavior.[18] Fast crosslinking helps minimize the effects of gravity and prevents the soft bioink from collapsing.

The biophysical considerations can be summarized: (1) The support matrix should reveal a Bingham plastic response; (2) The support matrix should liquify at physiologically relevant temperatures (37 °C), allowing for the non-destructive release of the printed constructs; (3) The aqueous phase of the matrix should support multiple independent crosslinking strategies, such as *p*H changes, divalent cations, and UV exposure, to gel different hydrogels and other soft polymeric materials. Extrusion within the support matrix can mitigate the effects of gravity, allowing for freeform printing of delicate constructs.[45]

2.4. Matrix rheology in FRESH

A key parameter specific to FRESH is the microparticle size, ranging from tens to hundreds of micrometers.[46] Microparticles of 25 μm diameters are ideal as they maintain their polydispersity and sphericity.[47] Smaller microparticles allow for higher-resolution 3D printing but may reduce mechanical stability. Larger microparticles provide better structural support but can limit the achievable resolution. The matrix shear-thinning enables the fluid to flow smoothly through the printing nozzle during deposition. The viscosity should be low enough to facilitate extrusion but high enough to prevent excessive spreading or collapse of the structure. The viscosity should be adjusted to ensure proper flow, allowing smooth extrusion through the nozzle while maintaining structural stability. For example, overall viscosity ranges from 5 to 30 Pascal-seconds (Pa s) for the gelatin matrix.[48]

The existing literature lacks comprehensive information regarding the rheological characteristics of matrices. To address this gap, we generated these matrices through mechanical blending, employing diverse concentrations and blend times, as discussed in the Experimental section. The resulting viscosity shear-rate responses obtained for the matrices prepared by blending 5–10% w/v gelatin matrices are shown in Fig. 2A, and by combining 2–4% w/v agarose matrices are demonstrated in Fig. 2B. The average size in Fig. 2C and D increases by the blend time or decreases by the gel concentration, which can improve the resolution. We observed that at blend times longer than 120 s (using a commercial blender), the gel particles began to dissolve and form a solution instead of a granular form; therefore, they could not be used in FRESH 3D bioprinting. To illustrate all rheological responses of the matrices, we illustrated two collective master curves for gelatin (Fig. 2E) and agarose matrices (Fig. 2F) by describing the variations of the shifted viscosity ($\beta\cdot\eta$) *versus* the shifted shear rate ($\alpha\cdot\dot{\gamma}$) in logarithmic scales. The master curves show a universal rheological landscape for the granular matrix methods. The calculation, interpretation, and utilization of the proposed master curves are discussed in the supplementary and the raw data is available in the ESI.†

2.5. Matrix-mediated crosslinking of deposited strands

Biomimetic natural biomaterials, such as collagen, fibronectin, alginate, gelatin, HA, and synthetic biopolymers, such as polyethylene glycol, polycaprolactone (PCL), and Pluronic, are among the most used cross-linkable bioinks (see Tables 1 and 2). Crosslinking can impact the behavior of biological components.[49] The ECM proteins crosslink and form stable hydrogels by an agent or post-processing steps. Alginate, a natural and biocompatible polymer, is crosslinkable in the presence of divalent cations, such as calcium, to form stable hydrogels, making it difficult to be printed directly. They create and maintain their shape by embedding alginate structures in the gelatin matrix with calcium ions. The high temperature melts away the gelatin support matrix and releases the alginate structures.[7] Hydrogels such as collagen and other decellularized ECM can also support the matrix with a pH buffer. HEPES, a zwitterionic buffer capable of maintaining a pH of 7.3–7.4, is used to supplement the support matrix for the embedded extrusion of collagen. As the collagen bioink is extruded into the HEPES-supplemented support matrix, the pH neutralization rapidly crosslinks the extruded collagen, driving the initial gelation process.

2.6. Extruding bioink requirements

The bioinks must shield cells from shear stresses during printing and offer non-toxic gelation for optimal resolution. The material's chemical composition, structural morphology, surface characteristics, surface charge, and mechanical properties can be modified to improve biocompatibility. The material must be capable of rapid crosslinking to ensure the layered formation of complex 3D structures. The bioink should possess suitable rheological properties to allow extrusion or deposition through the bioprinting nozzle while having the cells intact. The gelation kinetics of the bioink can be triggered by various mechanisms such as temperature, pH, light, or enzymatic reactions. Proper control of gelation kinetics ensures that the deposited bioink retains its shape.

Mechanical properties such as elasticity, stiffness, compressive strength, and elongation at break can be tailored to specific applications. The mechanical properties of hydrogel vary depending on concentration and cell density.[50] During printing, sacrificial materials with improved mechanical properties should be selected as support, especially for most natural polymers with intrinsically poor mechanical properties. Cell-loaded bioinks show reduced viscosity with increased cell concentration.[51] While fibrin shows viscosities between 2 and 162 mPa s, the blended bioink containing fibrin and HA shows viscosities between 100–1000 mPa s.[48] These properties determine the extrusion rate and printability of the bioinks.

Stability is another factor, as bioink should maintain its structure and stability during and after printing, which

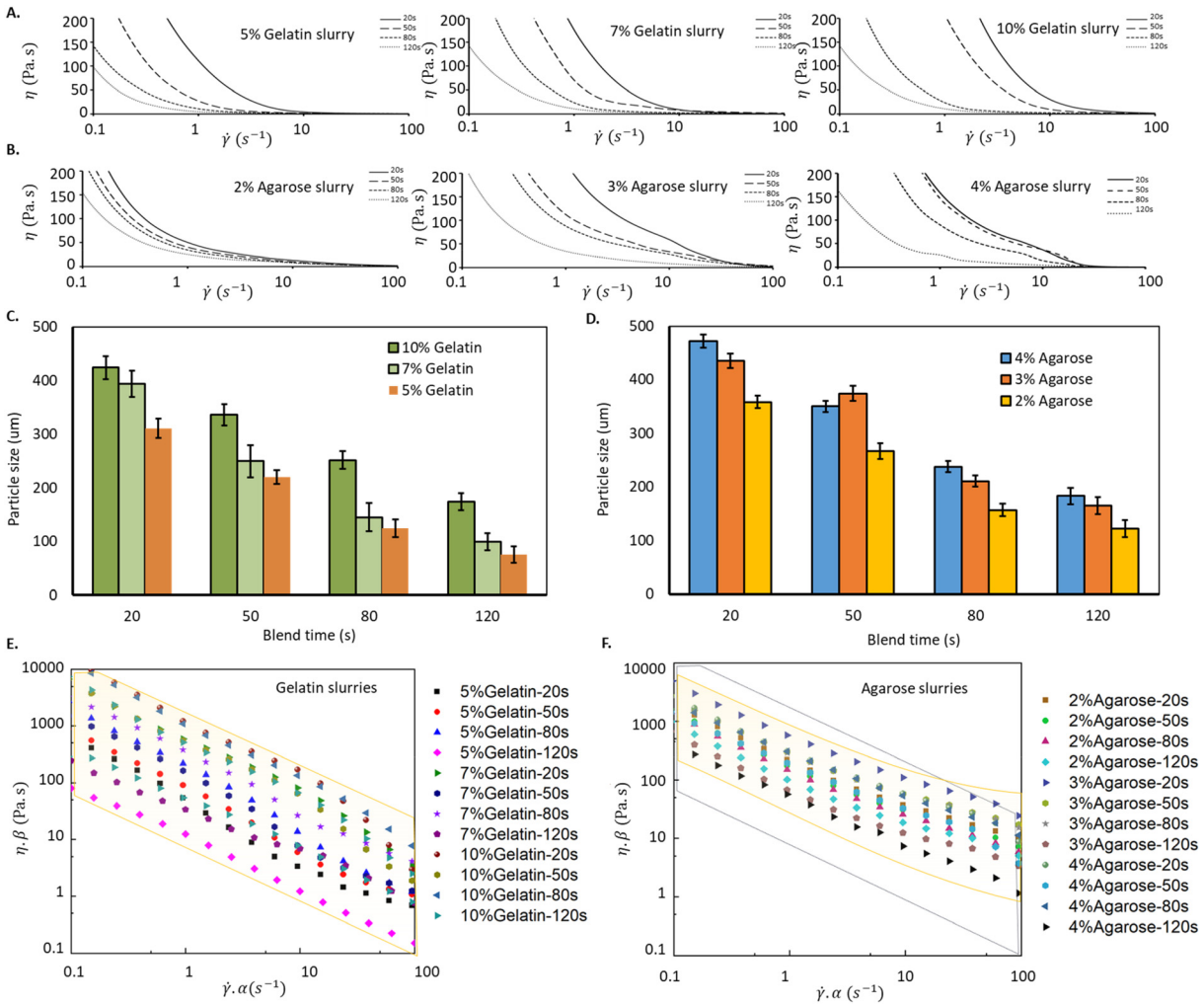

Fig. 2 FRESH-specific rheological response of different slurries made of (A) 5, 7, and 10% w/v gelatin and (B) 2, 3, and 4% w/v agarose, utilizing 20, 50, 80, and 120 s blend time; the average microparticle size obtained after blending the (C) gelatin and (D) agarose slurries; the calculated master curve locus obtained for (E) gelatin and (F) agarose slurries.

requires composition optimization, including the choice of matrix materials, crosslinking mechanisms, and rheology modifiers to ensure successful 3D bioprinting.[52] Sterilization is another step for implementing biomaterials, using a variety of processes, such as heat/steam treatment (autoclaving), e-beam or gamma irradiation, ethylene oxide treatment, incubating with ethanol, and other techniques to inactivate all forms of microbial life.

3. Bioink selection

3.1. Natural hydrogels

Table 2 summarizes natural bioinks and relevant support matrix for embedded extrusion 3D bioprinting. Alginate is a polysaccharide derived from brown seaweed and algae cell walls[53] and has ECM characteristics.[54] Pure alginate has low viscosity, which impacts its ability to retain its shape.[55] Alginate has low bioactivity and lacks cell-binding sites for cell proliferation.[56] It crosslinks and forms a gel in the presence of divalent cations such as calcium ions (Ca^{2+}).

Collagen is the most prevalent ECM molecule found in adult mammals, with an estimated 30% of the protein mass of multicellular organisms.[60] Under physiological conditions (7.4 pH and 37 °C), collagen molecules start to self-organize into fibrils, and collagen solution forms a hydrogel. Some studies used low-concentration collagen solutions from 5 mg ml^{-1} and rarely as high as 10 mg ml^{-1}.[61] One of the possible approaches to overcome this limitation is the use of supportive hydrogels. When using a supportive hydrogel for 3D bioprinting with collagen bioink, as seen in the FRESH method, the whole process occurs inside the secondary hydrogel matrix. This method allows printing complex structures using collagen solutions of low concentrations with a polymerization period of 40–60 min. For collagen type I at concentrations ranging from 8.94 to 9.64 mg ml^{-1} in 0.02 N acetic acid, the support matrix is supplemented with HEPES to maintain a pH of ~7.4 to ensure the crosslinking of collagen into a gel after extrusion.

Table 2 Selected extruding natural bioinks used for embedded extrusion 3D bioprinting

Ink	Cell type	Target	Crosslinking	Resolution	Advantages	Disadvantages	Ref.
Alginate	Fibroblasts, keratinocyt-es, hMSC, hASC	Bone and adipose tissue	Ionic-bonding	400 to 600 μm	Quick gelation, shape integrity, inexpensive, good stability	Rapid degradation, lacks cell-binding motifs, printer nozzle clogging	57
Collagen Type I	Fibroblasts, hMSCs, HUVECs, HEK, hiPSC-CMs	Skin, cardiac, liver, muscle	Hydrogen-bonding	1000 μm	Biodegradable, biocompatible, easily available, enhances cell adhesion factors like RGD	Low mechanical stability, poor gelation kinetics, expensive, low viscosity, limited sterilization	13
Fibrin	L929, hiPSC-CMs, NT2 neurons	cardiovascular tissue, nerve tissue	Enzymatic action of thrombin on fibrinogen	N/A	Good angiogenesis, fast gelation, soluble, biocompatible, biodegradable, robust	Fast biodegradation, irreversible gelation	58
Gelatin	Fibroblasts, mouse MSCs, immortalized glioblastoma cells, C2C12s, mouse MSCs	Brain, cardiac, skin	Covalent- and hydrogen-bonding	350 to 450 μm	Low antigenicity, inexpensive, reversible	Less stable at cell-friendly temperatures, poor mechanical properties	45
Silk fibroin	L929, porcine meniscal chondrocytes, human bone marrow MSCs	Meniscus tissue, skin	Hydrogen- and covalent-bonding	280 to 320 μm	Low cost, slow degradation, good mechanical properties, non-toxic	Lack cell binding domains, low cell viability, allergic response	59

HEPES neutralizes acetic acid. After printing, scaffolds are incubated at 37 °C for at least 1 hour to cross-link the collagen and melt the support bath.[62]

Fibrin is a native biopolymer formed during blood coagulation. Fibrin has RGD sequences that promote cell adhesion. It is physiologically biodegradable through plasmin-mediated fibrinolysis, which replaces fibrin by the ECM secreted by cells.[63] Fibrin can withstand high blood flow pressure, has a high elastic deformation capacity, and is large and stretchable, with an average breakage of >300% strain.[64] The mechanical properties of fibrin gel can be tuned by adjusting the concentrations of fibrinogen and thrombin, which affects the fibrin polymerization mechanism and stiffness. Hinton *et al.* reported that fibrinogen bioinks could form complex structures when printed in a gelatin support matrix supplemented with thrombin.[58]

Silk fibroin (SF) is a naturally derived protein obtained from Bombyx mori (B. mori) cocoons with excellent biocompatibility.[65] It is commonly used in surgical sutures for clinical applications and is degradable by proteolytic enzymes.[66] Gelation of silk can happen without any important secondary structural changes as intramolecular crosslinking between protein chains takes place with the aid of electrostatic interaction, hydrogen bonds, and hydrophobic interactions, forming strong β-sheets. The gelation time can be shortened with the aid of physical changes such as lowering the pH,[67] increasing the temperature,[68] sonication,[69] or adding chemical crosslinking agents.[70] Recombinant silk can be used for FRESH 3D bioprinting by letting a silk-cell mixture gel overnight before being used with extrusion printing.

The non-sulfated glycosaminoglycan HA is widely used in bioprinting due to its cytocompatibility, biological properties, and availability in chemical functionalization.[71] HA molecular weights range between 100 and 2500 kDa. HA polymer concentrations range from 0.1%–4% w/v (depending on the used molecular weight) with a large spectrum of mechanical properties and rates of biodegradation.[72] Pure and unmodified HA at working concentrations is unsuitable for producing printable inks. HA solutions show no yield stress and no shape retention upon printing. Therefore, rather than being printed alone, it is combined with other biomaterials, either natural or synthetic polymers, and thus can effectively be used with for embedded extrusion 3D bioprinting.

3.2. Synthetic polymers and photocrosslinkable bioinks

Synthetic bioinks used for embedded extrusion 3D bioprinting are summarized in Table 3. Poly(ethylene glycol) (PEG) is a hydrophilic, biocompatible, and water-soluble synthetic polymer that has been investigated in tissue engineering applications.[73] When combined with light-sensitive molecules, PEGDA-based biomaterial bioinks are among the most common systems for fabricating high-resolution constructs with stereolithography printing.[74] However, the limited protein binding sites on PEGDA lead to poor cell attachment on the printed PEGDA scaffolds, hindering its application. To overcome this obstacle, strategies of modifying PEGDA with cell-adhesive components such as hexapeptide and RGD peptides have enhanced cell survival, attachment, and spreading on the printed PEGDA scaffolds.[75] Pluronic is a block-copolymer consisting of a central poly (propylene oxide) (PPO) block flanked by poly (ethylene oxide) (PEO) blocks. Pluronic is a thermosensitive polymer with inverse thermo-gelling properties, *i.e.*, at low temperatures, a solution of Pluronic is liquid, whereas upon increasing the temperature, the solution forms a soft, physical gel. In the case of Pluronic F127 (PF127), gels can be formed below 37 °C for solutions above 14% w/v in the cell

Table 3 Summary of synthetic bioink systems used for embedded 3D bioprinting

Ink	Method	Cells	Target	Temp.	Resolution	Advantages	Disadvantages	Ref.
PDMS	Extrusion	No cell	Bone, cartilage	65 °C	100–400 μm	Optical transparency, high biocompatibility, moldability, submicron resolution	Lateral fusion of extruded PDMS filaments	15
PEG	Stereo-lithography	MSCs	Bone, cartilage	25 °C	10–100 μm	High transparency, tunable mechanical properties	Cytotoxicity, low cellular adhesion, and proliferation	78
PCL	Extrusion	hADSC, MSCs	Bone, Cartilage	60 °C	100–1000 μm	Good bioactivity, cells and hydrogels can be printed	Low accuracy	79
Pluronic F127	Extrusion	Chondrocytes	Cartilage	37 °C	150 μm	Reversible polymer	Cytotoxic	80

culture media.[76] These gels show shear thinning behavior[77] and good shear recovery, crucial for accurate 3D extrusion printing. Pluronic can also be used as the support matrix.

4. Applications of embedded extrusion 3D bioprinting

A 3D bioprinted tissue should have the following characteristics: (1) replicate the tissue-specific vascular networks in a certain size range (Fig. 3A and B), (2) possess sufficient mechanical properties that match the host tissue, (3) integrate with the body vascularization system to maintain tissue functions. The embedded extrusion method allows combining and optimizing strategies to induce *in vivo*-like characteristics for the 3D bioprinted tissue (Fig. 3C). For example, Fig. 3D illustrates a FRESH-printed perfusable full-size coronary artery composed of the artery lumen hollow. The coronary artery segment is 3D FRESH printed in alginate with a needle inserted at the proximal end, which, after perfusion, demonstrates bifurcation. The method has been successfully used to fabricate a full-size model of the adult human heart, showing that the model deforms similarly to a real heart. Sectioning the FRESH-3D-bioprinted aortic valves shows the notable internal structure resolution (Fig. 3Dviii).

4.1. Vascularized models

Printing large free-form tissue structures is often challenging due to soft hydrogel-based bioink's inadequate structural integrity and mechanical stability. The FRESH method has gained popularity for constructing complex freeform structures in a support matrix. The printed structures can be removed from the suspension medium by washing away the matrix after raising the temperature. A functional vascular network can maintain high cell viability in tissue-engineered scaffolds to deliver adequate nutrients and oxygen to the core of the grafts and promote tissue regeneration. Several methods have been explored and evaluated for the bioprinting of blood vessels. These methods attempt to mimic a native blood vessel function. Researchers have tried to include endothelial cells that line the inner walls of the tunica intima, smooth muscle cells of the tunica media, and a structural layer of 3T3 cells mimicking the tunica adventitia.[81] The endothelial cells perform several critical actions, including but not limited to maintaining the tunica intima, regulating vascular tone, and promoting antithrombotic activity. The tunica media of the large vessels contains elastin and elastic fibers.

Hinton *et al.* proposed the FRESH technique[15] and optimized support matrix to make filaments down to 20 μm in diameter and enabled direct printing of collagen, which usually requires some degree of modification or blending for vascular-like structures.[82–84] Among them, alginate hydrogel has been particularly attractive for creating vascular-like structures in tissue engineering and biomanufacturing due to its favorable properties, including biocompatibility, printability, and ease of gelation. In the method of using alginate-calcium ion crosslinking to fabricate vascular networks by using the FRESH method, the calcium ions must be added to the matrix during the liquid phase to initiate crosslinking and embed the extruded alginate structure. Studies have shown that although calcium ions promote cell growth, their varying concentrations may induce distinct cell behavior.

Skylar-Scott *et al.* developed the sacrificial writing into functional tissue (SWIFT) method in which a support matrix made of dense cellular spheroids sustains the printing of a gelatin sacrificial bioink. The authors demonstrated the bulk vascularized tissue function by creating a perfusable cardiac tissue that can fuse and beat synchronously over one week. Branched hierarchical vascular networks were endothelialized with HUVECs and enclosed in a compacted tissue construct. The main limitation was that to maintain high fidelity, the diameter of the sacrificial filaments needed to be ~400 μm, twice the size of the spheroids.[40] Since the sacrificial materials involved no cell, a high fabrication resolution could be achieved. However, the post-fabrication processes involving matrix removal and endothelial cells settling due to gravity were complicated and time-consuming, affecting cell viability within the tissues.[85] High-quality vascular networks need the encapsulated cells to have the same activities as their native counterparts. Integrating multiple cells within the vascular networks is necessary to achieve vascular functions. FRESH 3D bioprinting has already made it possible to print multiple types of cells simultaneously at a clinical size scale.

4.2. Large-scale tissue scaffolds

3D bioprinting of large-scale tissue scaffolds has been a challenge due to the structural complexities present while printing

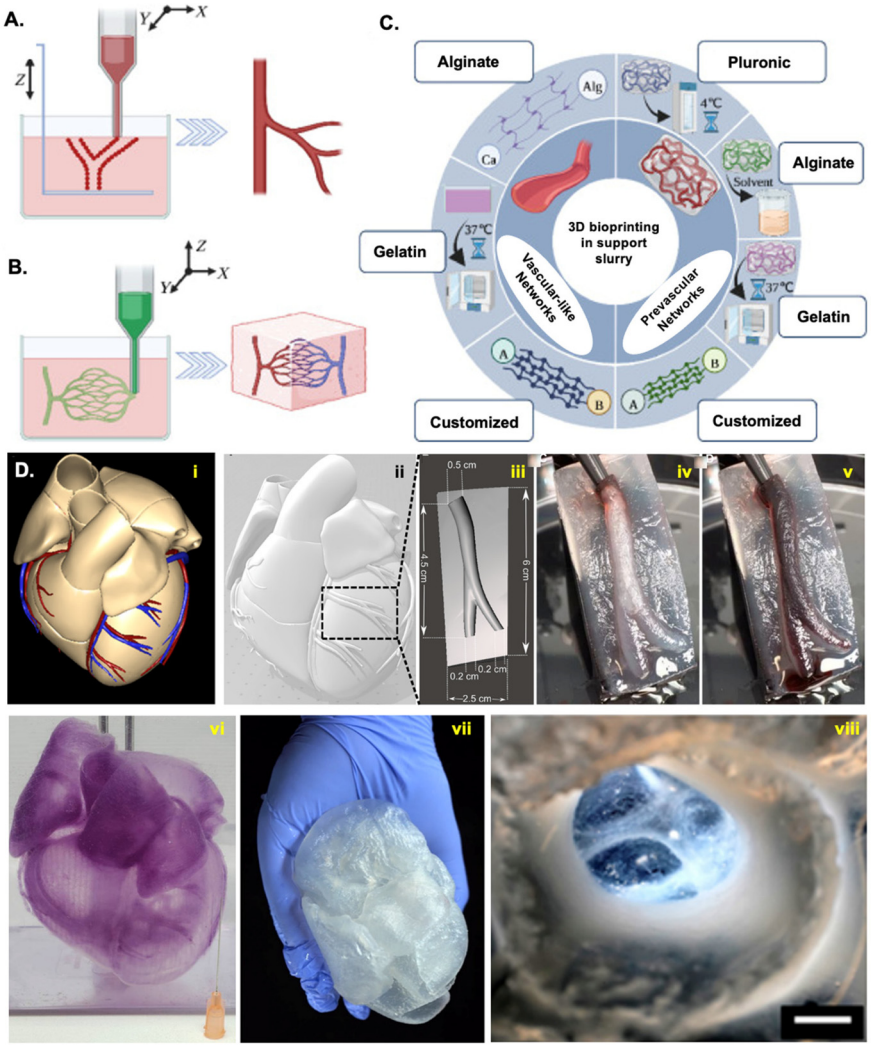

Fig. 3 (A) Vasculatures using embedded extrusion printing, (B) angiogenesis models using fugitive/sacrificial bioinks, (C) a review of different structures and slurry materials used in FRESH strategy, (D) a FRESH-printed perfusable full-size coronary artery (i), 3D scan of the human heart (ii), the model is segmented to isolate a region of a coronary artery superimposed on the left ventricle wall (iii), coronary artery was further processed to make the artery lumen hollow (vi), coronary artery segment in alginate with a needle inserted at the proximal end (v), coronary artery segment after perfusion with red glycerol demonstrating patency through the bifurcation (vi), a full-size adult human heart model and stained with a 0.1% (w/v) Alizarin red (vii), alginate heart (not stained) handled in the air to show that the model deforms similar to a real heart (vii), and sectioning the aortic valves to show the resolution (viii), the scale bar is 1 cm (adapted from ref. 45 with permission from American Chemical Society, copyright 2020).

in a layer-by-layer fashion. It is often challenging to print complex tissues or organs encompassing geometrical features such as branches, thin walls, and overhangs, as most hydrogels used as bioinks in bioprinting are too soft to provide adequate self-support.[86] To address this issue, the FRESH method can be used to provide a sacrificial support matrix to assist with extrusion. For example, Kang *et al.* used polycaprolactone (PCL) and Pluronic-F127 as the framework and sacrificial printing material, respectively, to support the printing of cell-laden composite hydrogels into complex human-tissue-scale constructs such as those for mandibles and ear cartilage.[79]

Biomimetic models such as human femurs are FRESH printed in alginate microparticle matrix (Fig. 4Ai,ii). The printed femur under uniaxial tensile testing demonstrates the ability to be strained up to 40% and elastically recover comparable to the natural femur (Fig. 4Aiii).[58] FRESH also enables printing a wide variety of low viscosity bioinks, such as collagen and decellularized ECM (dECM), which are necessary for the functional maturation of soft tissues.[87] Lee *et al.* used collagen bioink printed in shell layers to support the deposition of a high-concentration (3×10^8 ml^{-1}) cardiomyocyte suspension. They fabricated a cellular contracting model of the heart's left ventricle.[13] Noor *et al.* printed a miniaturized cellular heart model containing the major blood vessels by printing dECM-based bioinks in a hybrid support medium of calcium-alginate nanoparticles and xanthan gum.[32]

Bliley *et al.* FRESH 3D bioprinted a heart tube collagen bioink into a gelatin support matrix (Fig. 4Bii and iii) and cast

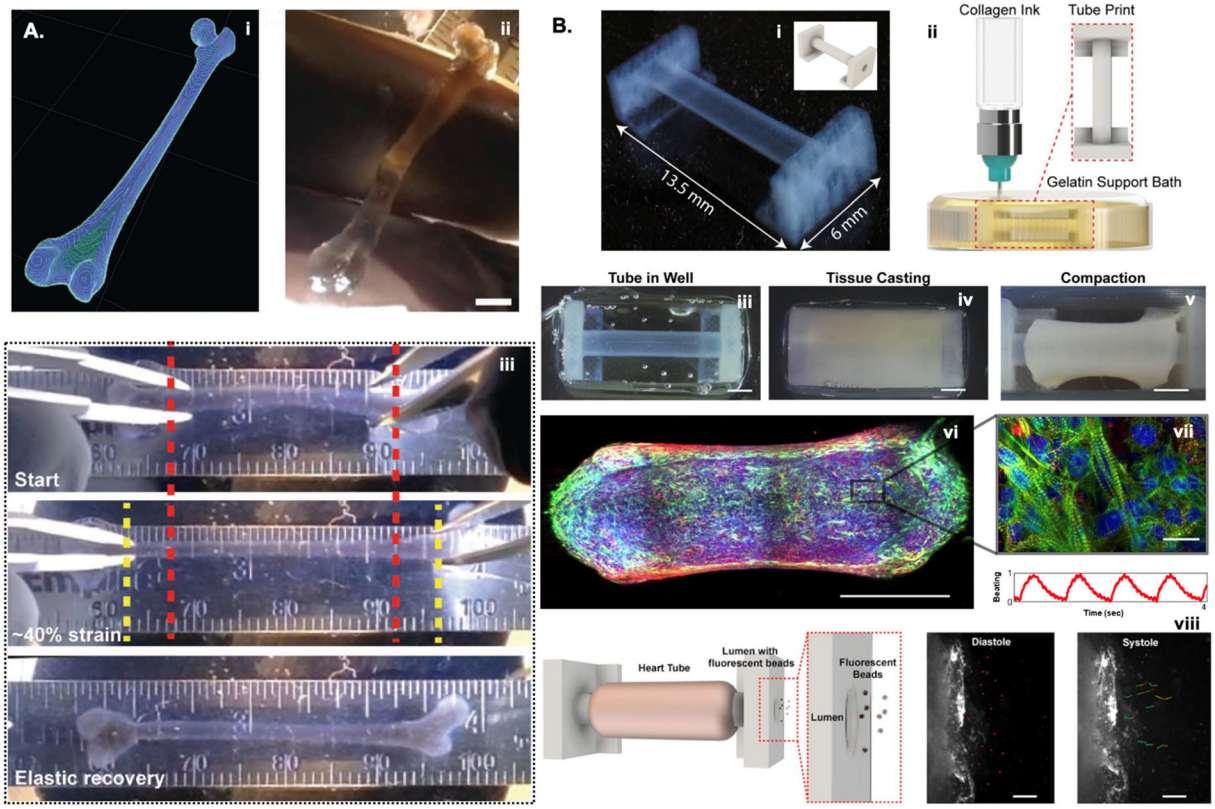

Fig. 4 Biomimetic models: (A) (i) a human femur model from 3D CT data is FRESH printed in alginate microparticle matrix, (ii) and after removal from the support matrix, it closely resembles the model and is easily handled, (iii) and uniaxial tensile testing of the printed femur demonstrates the ability to be strained up to 40% and elastically recover (adapted from ref. 58), (B) (i) isometric view of a linear heart tube model which is FRESH printed with collagen bioink into a gelatin support matrix; (ii and iii) the bioprinted hollow tube is placed in a PDMS cavity, (iv) then casted with cardiomyocytes and fibroblasts in a collagen mastermix, (v) the cast compacts after collagen polymerization, (vi) max intensity projection of heart tube surface shows cardiomyocytes positive for sarcomeric < actinin (red), actin (green), and DAPI (blue) > (inset: 2.5 mm), (vii) magnified images of the heart tube surface showing densely interconnected and striated cardiomyocytes (inset: 20 μm) and relative calcium fluorescent intensity with regular beating rate of the tissue at 1 Hz stimulation, (viii) fluorescent beads are displaced after tissue contraction at diastole and systole (scale bar: 300 μm, adopted from ref. 88 with permission from IOP Publishing, copyright 2009).

cardiomyocytes and fibroblasts in a collagen master. The heart tube showed densely interconnected cardiomyocytes and relative calcium fluorescent intensity at the center of the tissue with regular beating rate and tissue contraction at diastole and systole (Fig. 4vi and viii), demonstrating how the FRESH-3D-bioprinted heart tube can pump fluid similar to a heart muscle.[88] Integrating a vasculature system that supplies essential nutrients and oxygen to the cells while removing metabolic waste is a major hurdle in the bioprinting of large-scale tissue scaffolds. Lewis *et al*. developed a sacrificial printing strategy of simultaneously printing cell-laden bioink and sacrificial bioink to create a vascularized tissue.[89] Another strategy has been the omnidirectional bioprinting technique in a suspension matrix. More biomimicry has been achieved as it enables layer-by-layer deposition of the bioink. FRESH 3D bioprinting is a cell-compatible platform to produce complex three-dimensional geometries using cell-laden bioinks. Several challenges persist when cellularizing a tissue construct at full organ size. The first hurdle is the long duration of the printing process, where some models take more than four days to complete. The next challenge is the cost of biomaterials and the requirement for culturing billions of cells for the cell seeding process.

5. Future directions

There is a current trend to use embedded extrusion 3D bioprinting methods to create non-temporary matrices. There is a need for crosslinkers that can work with various bioinks. Hull *et al.*[90] created bioinks where polysaccharides, protein, and manufactured spine polymers were utilized to form bioinks crosslinked by a common "click chemistry" where numerous materials can be printed together to create a bound-together scaffold (see Fig. 1B). Physical crosslinking can include the addition of metal ions or photoinitiators to the bioink solution, applying electromagnetic fields or stress/force, and controlling temperature. For example, in collagen, a gelatin matrix is supplemented with a zwitterionic buffer, HEPES, allowing for crosslinking the extruded collagen material while supporting cells in the bioink.[45] The tempera-

Table 4 Future directions in embedded extrusion 3D bioprinting

Future direction	Description	Expected impact
Advanced materials development	Developing bioinks with high resolution and biocompatibility, as well as crosslinkers that can work with various bioinks to create non-temporary matrices and support bath for FRESH bioprinting	Enhanced precision and cell viability in printed tissues
Enhanced printing techniques	Implementing multi-material printing and merging different types of extrusion and stereolithography based techniques with FRESH bioprinting. Moreover, utilizing automation and AI for precision and efficiency	Creating more complex and functional tissue constructs
Optimization of sacrificial support matrices	Fine-tuning rheological properties and developing biodegradable matrices with predictable Brigham plastic flow behavior especially for *in vivo* biofabrication	Improved support during printing and *in vivo* applications
Scalability and standardization	Scaling up production and establishing regulatory standards for clinical grade bioprinting of thick tissues and organs	Wider adoption and clinical application

ture of the support matrix is then raised to 37 °C for thermal crosslinking as an additional condition for accelerating collagen polymerization while melting away the support gelatin matrix.

Another form of physical crosslinking is photocrosslinking. An excellent example of photocrosslinking is *via* creating the photopolymer GelMA with an ideal concentration of GelMA 5–15% (w/v).[91] The gelling/liquefying points identified are 24 °C and 26 °C for 5% and 10% GelMA solutions, respectively. To address the issues of long gelation time and poor mechanical and degradation properties of GelMA, the FRESH 3D bioprinting method can be used to directly bioprint GelMA into the support matrix. This is followed by photo-crosslinking under UV light, enabling the fabrication of complex 3D constructs.[92] The support matrix is illuminated with UV light, which crosslinks the extruded photosensitive biomaterial held within the matrix. An optimal threshold or balance exists between the degree of crosslinking and the resulting structure. A low degree of crosslinking may cause the bioink to disperse within the matrix.

A high degree of crosslinking may cause blockage in the extruder needle, preventing the material from being printed. Some of the crosslinking methods may have effects on cell viability and behavior in bioink. Photocrosslinkers such as UV irradiation may provide the added advantage of sterilization by killing micro-organisms, but exposure to light irradiation or to free radicals generated from photoinitiators can increase the risk of phototoxicity or DNA damage and thus can influence the functionality of the cell-laden printed construct.[93] The matrix is translucent, and the size of the support matrix and the printed structure will affect the amount of UV light penetration. The UV light source is generally placed outside the support matrix. This means not all matrix parts will receive the same amount of irradiation, further affecting cross-linking quality during printing. Other limitations include the non-uniform mixing of the supplemented crosslinkers in the gelatin matrix, which may cause non-uniform crosslinking of the printed structure. Table 4 summarizes some future directions in developing embedded extrusion 3D bioprinting.

Embedded extrusion can include other methods, such as the hierarchical assembly of silk fibroin in 3D macroscale architectures with inherent biocompatibility, mechanical robustness, and desired geometry. Mu *et al.* tweaked the composition of salt ions (0.5 M of dipotassium phosphate and 4 M of sodium chloride) in an aqueous bath to direct silk fibroin assembly. The salt bath recapitulated native spinning solvent conditions, including dehydration, acidification, and ionic gradients.[94–96] This method allowed for monolithic protein composition and improved mechanical performance resulting from the salt-directed hierarchical molecular assembly.

Author contributions

S.Y.: writing – original draft preparation, data curation, validation; H.G.H: writing – reviewing and editing, methodology, investigation; D.E.G: investigation; A.K.M.: writing – original draft preparation, reviewing and editing, supervision, funding acquisition.

Data availability

The rheological data supporting this article (Fig. 2) have been included as part of the ESI.†

Conflicts of interest

The authors declare no conflict of interest.

Acknowledgements

We thank federal agencies for their support (NSF-2243506 and NIH-R01DC018577) and Mr Luis M. Medina (Advanced Biofabrication Lab, NJIT) for his contributions to collecting raw rheometry data.

References

1 A. K. Miri, *et al.*, Bioprinters for organs-on-chips, *Biofabrication*, 2019, **11**(4), 042002.

2 H. Goodarzi Hosseinabadi, *et al.*, Digital Light Processing Bioprinting Advances for Microtissue Models, *ACS Biomater. Sci. Eng.*, 2022, **8**(4), 1381–1395.

3 B. Cecen, *et al.*, Selection of natural biomaterials for micro–tissue and organ–on–chip models, *J. Biomed. Mater. Res., Part A*, 2022, **110**(5), 1147–1165.

4 K. J. Wolf, *et al.*, Biomanufacturing human tissues via organ building blocks, *Cell Stem Cell*, 2022, **29**(5), 667–677.

5 J. S. Liu and Z. J. Gartner, Directing the assembly of spatially organized multicomponent tissues from the bottom up, *Trends Cell Biol.*, 2012, **22**(12), 683–691.

6 A. Shapira, *et al.*, Stabilization strategies in extrusion-based 3D bioprinting for tissue engineering, *Appl. Phys. Rev.*, 2018, **5**(4), DOI: **10.1063/1.5055659**.

7 A. Schwab, *et al.*, Printability and Shape Fidelity of Bioinks in 3D Bioprinting, *Chem. Rev.*, 2020, **120**(19), 11028–11055.

8 A. K. Miri, *et al.*, Multiscale Bioprinting of Vascularized Models, *Biomaterials*, 2019, **198**, 204–216.

9 D. J. Shiwarski, *et al.*, Emergence of FRESH 3D printing as a platform for advanced tissue biofabrication, *APL Bioeng.*, 2021, **5**(1), 010904.

10 K. Hajash, B. Sparrman, C. Guberan, J. Laucks and S. Tibbits, Large-Scale Rapid Liquid Printing, *3D Print. Addit. Manuf.*, 2017, **4**, 123–132.

11 Y. Zhao, *et al.*, Process planning strategy for wire-arc additive manufacturing: Thermal behavior considerations, *Addit. Manuf.*, 2020, **32**, 100935.

12 Y. Jin, *et al.*, Functional Nanoclay Suspension for Printing-Then-Solidification of Liquid Materials, *ACS Appl. Mater. Interfaces*, 2017, **9**(23), 20057–20066.

13 A. Lee, *et al.*, 3D bioprinting of collagen to rebuild components of the human heart, *Science*, 2019, **365**, 482–487.

14 Q. Wu, *et al.*, Embedded extrusion printing in yield-stress-fluid baths, *Matter*, 2022, **5**(11), 3775–3806.

15 T. J. Hinton, *et al.*, 3D Printing PDMS Elastomer in a Hydrophilic Support Bath via Freeform Reversible Embedding, *ACS Biomater. Sci. Eng.*, 2016, **2**(10), 1781–1786.

16 M. Rocca, *et al.*, Embedded Multimaterial Extrusion Bioprinting, *SLAS Technol.*, 2018, **23**(2), 154–163.

17 M. Bohorquez, C. Koch, T. Trygstad and N. Pandit, A Study of the Temperature Dependent Micellization of Pluronic F127, *J. Colloid Interface Sci.*, 1999, **216**(1), 34–40. ISSN 0021-9797.

18 M. E. Cooke and D. H. Rosenzweig, The rheology of direct and suspended extrusion bioprinting, *APL Bioeng.*, 2021, **5**(1), 011502.

19 F. Afghah, *et al.*, Preparation and characterization of nanoclay-hydrogel composite support-bath for bioprinting of complex structures, *Sci. Rep.*, 2020, **10**(1), 5257.

20 H. Ding and R. Chang, Printability Study of Bioprinted Tubular Structures Using Liquid Hydrogel Precursors in a Support Bath, *Appl. Sci.*, 2018, **8**(3), 403.

21 O. Jeon, *et al.*, Individual cell-only bioink and photocurable supporting medium for 3D printing and generation of engineered tissues with complex geometries, *Mater. Horiz.*, 2019, **6**(8), 1625–1631.

22 A. McCormack, *et al.*, 3D Printing in Suspension Baths: Keeping the Promises of Bioprinting Afloat, *Trends Biotechnol.*, 2020, **38**(6), 584–593.

23 Z. Gu, *et al.*, Development of 3D bioprinting: From printing methods to biomedical applications, *Asian J. Pharm. Life Sci.*, 2020, **15**(5), 529–557.

24 A. M. Compaan, K. Song and Y. Huang, Gellan Fluid Gel as a Versatile Support Bath Material for Fluid Extrusion Bioprinting, *ACS Appl. Mater. Interfaces*, 2019, **11**(6), 5714–5726.

25 D. F. Duarte Campos, *et al.*, Three-dimensional printing of stem cell-laden hydrogels submerged in a hydrophobic high-density fluid, *Biofabrication*, 2013, **5**(1), 015003.

26 A. K. Grosskopf, *et al.*, Viscoplastic Matrix Materials for Embedded 3D Printing, *ACS Appl. Mater. Interfaces*, 2018, **10**(27), 23353–23361.

27 Y. Jin, W. Chai and Y. Huang, Printability study of hydrogel solution extrusion in nanoclay yield-stress bath during printing-then-gelation biofabrication, *Mater. Sci. Eng., C*, 2017, **80**, 313–325.

28 Y. Jin, *et al.*, Granular gel support-enabled extrusion of three-dimensional alginate and cellular structures, *Biofabrication*, 2016, **8**(2), 025016.

29 S. G. Patricio, *et al.*, Freeform 3D printing using a continuous viscoelastic supporting matrix, *Biofabrication*, 2020, **12**(3), 035017.

30 K. H. Song, *et al.*, Complex 3D–Printed Microchannels within Cell–Degradable Hydrogels, *Adv. Funct. Mater.*, 2018, **28**(31), 1801331.

31 D. J. Shiwarski, *et al.*, Emergence of FRESH 3D printing as a platform for advanced tissue biofabrication, *APL Bioeng.*, 2021, **5**(1), 010904.

32 N. Noor, *et al.*, 3D Printing of Personalized Thick and Perfusable Cardiac Patches and Hearts, *Adv. Sci.*, 2019, **6**(11), 1900344.

33 M. Machour, *et al.*, Print-and-Grow within a Novel Support Material for 3D Bioprinting and Post-Printing Tissue Growth, *Adv. Sci.*, 2022, **9**(34), e2200882.

34 J. J. Senior, *et al.*, Fabrication of Complex Hydrogel Structures Using Suspended Layer Additive Manufacturing (SLAM), *Adv. Funct. Mater.*, 2019, **29**(49), 1904845.

35 J. Kajtez, *et al.*, Embedded 3D Printing in Self-Healing Annealable Composites for Precise Patterning of Functionally Mature Human Neural Constructs, *Adv. Sci.*, 2022, **9**(25), e2201392.

36 L. Ning, *et al.*, A 3D Bioprinted in vitro Model of Neuroblastoma Recapitulates Dynamic Tumor-Endothelial Cell Interactions Contributing to Solid Tumor Aggressive Behavior, *Adv. Sci.*, 2022, **9**(23), e2200244.

37 M. O. Ozturk-Oncel, *et al.*, A dive into the bath: embedded 3D bioprinting of freeform in vitro models, *Biomater. Sci.*, 2023, **11**(16), 5462–5473.

38 Y. Yu, *et al.*, Vascular network-inspired fluidic system (VasFluidics) with spatially functionalizable membranous walls, *Nat. Commun.*, 2024, **15**(1), 1437.

39 G. Luo, *et al.*, Freeform, Reconfigurable Embedded Printing of All-Aqueous 3D Architectures, *Adv. Mater.*, 2019, **31**(49), e1904631.

40 M. A. Skylar-Scott, S. G. M. Uzel, L. L. Nam, J. H. Ahrens, R. L. Truby, S. Damaraju and J. A. Lewis, Biomanufacturing of organ-specific tissues with high cellular density and embedded vascular channels, *Sci. Adv.*, 2019, **5**(9), eaaw2459.

41 W. W. Cho, *et al.*, Blood-Lymphatic Integrated System with Heterogeneous Melanoma Spheroids via In-Bath Three-Dimensional Bioprinting for Modelling of Combinational Targeted Therapy, *Adv. Sci.*, 2022, **9**(29), e2202093.

42 G. Gao, *et al.*, Construction of a Novel In Vitro Atherosclerotic Model from Geometry–Tunable Artery Equivalents Engineered via In–Bath Coaxial Cell Printing, *Adv. Funct. Mater.*, 2020, **31**(10), 2008878.

43 A. Malekpour and X. Chen, Printability and Cell Viability in Extrusion-Based Bioprinting from Experimental, Computational, and Machine Learning Views, *J. Funct. Biomater.*, 2022, **13**(2), 40.

44 E. Mirdamadi, *et al.*, Agarose Slurry as a Support Medium for Bioprinting and Culturing Freestanding Cell-Laden Hydrogel Constructs, *3D Print. Addit. Manuf.*, 2019, **6**(3), 158–164.

45 E. Mirdamadi, *et al.*, FRESH 3D Bioprinting a Full-Size Model of the Human Heart, *ACS Biomater. Sci. Eng.*, 2020, **6**(11), 6453–6459.

46 C. A. Wu, *et al.*, Optimization of Freeform Reversible Embedding of Suspended Hydrogel Microspheres for Substantially Improved Three-Dimensional Bioprinting Capabilities, *Tissue Eng., Part C*, 2023, **29**(3), 85–94.

47 L. Bova, F. Billi and E. Cimetta, Mini-review: advances in 3D bioprinting of vascularized constructs, *Biol. Direct*, 2020, **15**(1), 22.

48 F. Kreimendahl, *et al.*, FRESH bioprinting technology for tissue engineering – the influence of printing process and bioink composition on cell behavior and vascularization, *J. Appl. Biomater. Funct. Mater.*, 2021, **19**, 22808000211028808.

49 A. GhavamiNejad, *et al.*, Crosslinking Strategies for 3D Bioprinting of Polymeric Hydrogels, *Small*, 2020, **16**(35), e2002931.

50 R. Schwartz, *et al.*, Cell encapsulation in gelatin bioink impairs 3D bioprinting resolution, *J. Mech. Behav. Biomed. Mater.*, 2020, **103**, 103524.

51 E. Dogan, *et al.*, Cell encapsulation in gelatin methacryloyl bioinks impairs microscale diffusion properties, *Front. Bioeng. Biotechnol.*, 2023, **11**, 1193970.

52 L. Ning, *et al.*, Embedded 3D Bioprinting of Gelatin Methacryloyl-Based Constructs with Highly Tunable Structural Fidelity, *ACS Appl. Mater. Interfaces*, 2020, **12**(40), 44563–44577.

53 K. Y. Lee and D. J. Mooney, Alginate: properties and biomedical applications, *Prog. Polym. Sci.*, 2012, **37**(1), 106–126.

54 C. Benwood, *et al.*, Natural Biomaterials and Their Use as Bioinks for Printing Tissues, *Bioengineering*, 2021, **8**(2), 27.

55 J. Lee, *et al.*, Bone-derived dECM/alginate bioink for fabricating a 3D cell-laden mesh structure for bone tissue engineering, *Carbohydr. Polym.*, 2020, **250**, 116914.

56 M. Muller, *et al.*, Alginate Sulfate-Nanocellulose Bioinks for Cartilage Bioprinting Applications, *Ann. Biomed. Eng.*, 2017, **45**(1), 210–223.

57 H. H. Mishbak, G. Cooper and P. J. Bartolo, Development and characterization of a photocurable alginate bioink for three-dimensional bioprinting, *Int. J. Bioprint.*, 2019, **5**(2), 189.

58 T. J. Hinton, *et al.*, Three-dimensional printing of complex biological structures by freeform reversible embedding of suspended hydrogels, *Sci. Adv.*, 2015, **1**(9), e1500758.

59 M. J. Rodriguez, *et al.*, 3D freeform printing of silk fibroin, *Acta Biomater.*, 2018, **71**, 379–387.

60 C. Frantz, K. M. Stewart and V. M. Weaver, The extracellular matrix at a glance, *J. Cell Sci.*, 2010, **123**(Pt 24), 4195–4200.

61 H. Yoon, *et al.*, Development of cell-laden 3D scaffolds for efficient engineered skin substitutes by collagen gelation, *RSC Adv.*, 2016, **6**(26), 21439–21447.

62 S. Li, *et al.*, 3D bioprinting vascular networks in suspension baths, *Appl. Mater. Today*, 2023, **30**, 101729.

63 K. A. Ahmann, *et al.*, Fibrin degradation enhances vascular smooth muscle cell proliferation and matrix deposition in fibrin-based tissue constructs fabricated in vitro, *Tissue Eng., Part A*, 2010, **16**(10), 3261–3270.

64 W. Liu, L. M. Jawerth, E. A. Sparks, M. R. Falvo, R. R. Hantgan, R. Superfine, S. T. Lord and M. Guthold, Fibrin fibers have extraordinary extensibility and elasticity, *Science*, 2006, **313**(5787), 634.

65 Y. Qi, *et al.*, A Review of Structure Construction of Silk Fibroin Biomaterials from Single Structures to Multi-Level Structures, *Int. J. Mol. Sci.*, 2017, **18**(3), 237.

66 Y. Cao and B. Wang, Biodegradation of silk biomaterials, *Int. J. Mol. Sci.*, 2009, **10**(4), 1514–1524.

67 X. Tang, X. Qiao and K. Sun, Effect of pH on the interfacial viscoelasticity and stability of the silk fibroin at the oil/water interface, *Colloids Surf., A*, 2015, **486**, 86–95.

68 K. Schacht, *et al.*, Biofabrication of cell-loaded 3D spider silk constructs, *Angew. Chem., Int. Ed.*, 2015, **54**(9), 2816–2820.

69 M. Kumar, *et al.*, Immuno-Informed 3D Silk Biomaterials for Tailoring Biological Responses, *ACS Appl. Mater. Interfaces*, 2016, **8**(43), 29310–29322.

70 W. H. Elliott, *et al.*, Silk Hydrogels of Tunable Structure and Viscoelastic Properties Using Different Chronological Orders of Genipin and Physical Cross-Linking, *ACS Appl. Mater. Interfaces*, 2015, **7**(22), 12099–12108.

71 G. D. Prestwich, Hyaluronic acid-based clinical biomaterials derived for cell and molecule delivery in regenerative medicine, *J. Controlled Release*, 2011, **155**(2), 193–199.

72 J. A. Burdick and G. D. Prestwich, Hyaluronic acid hydrogels for biomedical applications, *Adv. Mater.*, 2011, **23**(12), H41–H56.

73 M. Lee, *et al.*, Guiding Lights: Tissue Bioprinting Using Photoactivated Materials, *Chem. Rev.*, 2020, **120**(19), 10950–11027.

74 H. Goodarzi Hosseinabadi, *et al.*, Ink material selection and optical design considerations in DLP 3D printing, *Appl. Mater. Today*, 2023, **30**, 101721.

75 J. Zhu, J. A. Beamish, C. Tang, K. Kottke-Marchant and R. E. Marchant, *Macromolecules*, 2006, **39**(4), 1305–1307.

76 J. E. Matthew, Y. L. Nazario, S. C. Roberts and S. R. Bhatia, Effect of mammalian cell culture medium on the gelation properties of Pluronic F127, *Biomaterials*, 2002, **23**(23), 4615–4619.

77 K. Hyun, *et al.*, Large amplitude oscillatory shear behavior of PEO-PPO-PEO triblock copolymer solutions, *Rheol. Acta*, 2005, **45**(3), 239–249.

78 C. Yu, *et al.*, Photopolymerizable Biomaterials and Light-Based 3D Printing Strategies for Biomedical Applications, *Chem. Rev.*, 2020, **120**(19), 10695–10743.

79 H. W. Kang, *et al.*, A 3D bioprinting system to produce human-scale tissue constructs with structural integrity, *Nat. Biotechnol.*, 2016, **34**(3), 312–319.

80 M. Müller, *et al.*, Nanostructured Pluronic hydrogels as bioinks for 3D bioprinting, *Biofabrication*, 2015, **7**(3), 035006.

81 J. Halper, Basic Components of Vascular Connective Tissue and Extracellular Matrix, *Adv. Pharmacol.*, 2018, **81**, 95–127.

82 D. F. Duarte Campos, *et al.*, Exploring Cancer Cell Behavior In Vitro in Three-Dimensional Multicellular Bioprintable Collagen-Based Hydrogels, *Cancers*, 2019, **11**(2), 180.

83 H. Stratesteffen, *et al.*, GelMA-collagen blends enable drop-on-demand 3D printablility and promote angiogenesis, *Biofabrication*, 2017, **9**(4), 045002.

84 F. Kreimendahl, *et al.*, Three-Dimensional Printing and Angiogenesis: Tailored Agarose-Type I Collagen Blends Comprise Three-Dimensional Printability and Angiogenesis Potential for Tissue-Engineered Substitutes, *Tissue Eng., Part C*, 2017, **23**(10), 604–615.

85 I. S. Kinstlinger, *et al.*, Perfusion and endothelialization of engineered tissues with patterned vascular networks, *Nat. Protoc.*, 2021, **16**(6), 3089–3113.

86 J. Groll, *et al.*, A definition of bioinks and their distinction from biomaterial inks, *Biofabrication*, 2018, **11**(1), 013001.

87 S. Lee, *et al.*, Human-Recombinant-Elastin-Based Bioinks for 3D Bioprinting of Vascularized Soft Tissues, *Adv. Mater.*, 2020, **32**(45), e2003915.

88 J. Bliley, *et al.*, FRESH 3D bioprinting a contractile heart tube using human stem cell-derived cardiomyocytes, *Biofabrication*, 2022, **14**(2), 4106.

89 D. B. Kolesky, *et al.*, Three-dimensional bioprinting of thick vascularized tissues, *Proc. Natl. Acad. Sci. U. S. A.*, 2016, **113**(12), 3179–3184.

90 S. M. Hull, *et al.*, 3D Bioprinting using UNIversal Orthogonal Network (UNION) Bioinks, *Adv. Funct. Mater.*, 2021, **31**(7), 2007983.

91 N. B. Allen, *et al.*, 3D-bioprinted GelMA-gelatin-hydroxyapatite osteoblast-laden composite hydrogels for bone tissue engineering, *Bioprinting*, 2022, **26**, e00196.

92 S. Das and B. Basu, An Overview of Hydrogel-Based Bioinks for 3D Bioprinting of Soft Tissues, *J. Indian Inst. Sci.*, 2019, **99**(3), 405–428.

93 M. Kazemzadeh-Narbat, *et al.*, Engineering Photocrosslinkable Bicomponent Hydrogel Constructs for Creating 3D Vascularized Bone, *Adv. Healthc. Mater.*, 2017, **6**(10), 1601122.

94 C. Guo, *et al.*, Engineering Silk Materials: From Natural Spinning to Artificial Processing, *Appl. Phys. Rev.*, 2020, **7**(1), 011313.

95 X. Mu, *et al.*, A brief review on the mechanisms and approaches of silk spinning-inspired biofabrication, *Front. Bioeng. Biotechnol.*, 2023, **11**, 1252499.

96 X. Mu, V. Fitzpatrick and D. L. Kaplan, From Silk Spinning to 3D Printing: Polymer Manufacturing using Directed Hierarchical Molecular Assembly, *Adv. Healthc. Mater.*, 2020, **9**(15), e1901552.